3-3-2020

Defining stage-specific activity of potent new inhibitors of Cryptosporidium parvum growth in vitro

Lisa J Funkhouser-Jones

Soumya Ravindran

L. David Sibley

AMERICAN SOCIETY FOR MICROBIOLOGY | mBio®

RESEARCH ARTICLE
Host-Microbe Biology

Defining Stage-Specific Activity of Potent New Inhibitors of *Cryptosporidium parvum* Growth *In Vitro*

Lisa J. Funkhouser-Jones,[a] Soumya Ravindran,[a] L. David Sibley[a]

[a]Department of Molecular Microbiology, Washington University School of Medicine, St. Louis, Missouri, USA

ABSTRACT *Cryptosporidium parvum* and *Cryptosporidium hominis* have emerged as major enteric pathogens of infants in the developing world, in addition to their known importance in immunocompromised adults. Although there has been recent progress in identifying new small molecules that inhibit *Cryptosporidium* sp. growth *in vitro* or in animal models, we lack information about their mechanism of action, potency across the life cycle, and cidal versus static activities. Here, we explored four potent classes of compounds that include inhibitors that likely target phosphatidylinositol 4 kinase (PI4K), phenylalanine-tRNA synthetase (PheRS), and several potent inhibitors with unknown mechanisms of action. We utilized monoclonal antibodies and gene expression probes for staging life cycle development to define the timing of when inhibitors were active during the life cycle of *Cryptosporidium parvum* grown *in vitro*. These different classes of inhibitors targeted different stages of the life cycle, including compounds that blocked replication (PheRS inhibitors), prevented the segmentation of daughter cells and thus blocked egress (PI4K inhibitors), or affected sexual-stage development (a piperazine compound of unknown mechanism). Long-term cultivation of *C. parvum* in epithelial cell monolayers derived from intestinal stem cells was used to distinguish between cidal and static activities based on the ability of parasites to recover from treatment. Collectively, these approaches should aid in identifying mechanisms of action and for designing *in vivo* efficacy studies based on time-dependent concentrations needed to achieve cidal activity.

IMPORTANCE Currently, nitazoxanide is the only FDA-approved treatment for cryptosporidiosis; unfortunately, it is ineffective in immunocompromised patients, has varied efficacy in immunocompetent individuals, and is not approved in infants under 1 year of age. Identifying new inhibitors for the treatment of cryptosporidiosis requires standardized and quantifiable *in vitro* assays for assessing potency, selectivity, timing of activity, and reversibility. Here, we provide new protocols for defining which stages of the life cycle are susceptible to four highly active compound classes that likely inhibit different targets in the parasite. We also utilize a newly developed long-term culture system to define assays for monitoring reversibility as a means of defining cidal activity as a function of concentration and time of treatment. These assays should provide valuable *in vitro* parameters to establish conditions for efficacious *in vivo* treatment.

KEYWORDS cryptosporidiosis, enteric pathogen, target identification, small-molecule inhibitors, intestinal stem cells, primary cell culture, mechanism of action

Cryptosporidiosis is a debilitating diarrheal disease in humans that is largely caused by two species, *Cryptosporidium parvum*, a zoonotic species acquired primarily from agricultural animals that can also transmit between humans, and the anthroponotic *Cryptosporidium hominis* species, which is almost exclusively transmitted from human to human (1). Infections are most severe in immunocompromised patients (2) and infants under age 2, particularly in developing countries (3). Unfortunately, the only

Citation Funkhouser-Jones LJ, Ravindran S, Sibley LD. 2020. Defining stage-specific activity of potent new inhibitors of *Cryptosporidium parvum* growth *in vitro*. mBio 11:e00052-20. https://doi.org/10.1128/mBio.00052-20.

Editor Louis M. Weiss, Albert Einstein College of Medicine

Address correspondence to L. David Sibley, sibley@wustl.edu.

This article is a direct contribution from L. David Sibley, a Fellow of the American Academy of Microbiology, who arranged for and secured reviews by Gary Ward, University of Vermont, and Michael Arrowood, Centers for Disease Control.

Received 10 January 2020
Accepted 16 January 2020
Published 3 March 2020

FDA-approved drug for the treatment of cryptosporidiosis, nitazoxanide, is largely ineffective in the most susceptible patient populations and is not licensed for infants under 1 year of age (4, 5). The identification of new compounds that inhibit *C. parvum* is hampered by the difficulty of *in vitro* propagation combined with animal models limited to immunocompromised mice (*C. parvum*), gnotobiotic piglets (*C. hominis*), or calves (*C. parvum*) (6).

Recent efforts have leveraged high-throughput screening platforms and repurposing screens to identify new compounds with the potential for advancement to clinical trials. A high-throughput screen of almost 80,000 small molecules identified 12 anticryptosporidial compounds that inhibit growth in the submicromolar range, including clofazimine (7). Screening of the open-access Malaria Box of compounds available through the Medicine for Malaria Venture (https://www.mmv.org/) identified a piperazine-based inhibitor (i.e., MMV665917) that showed potent activity in a NOD SCID gamma immunocompromised mouse model of chronic cryptosporidiosis (8), in neonatal dairy calves (9), and in gnotobiotic piglets infected with *C. hominis* (10). Screening of a focused library of antimalarial compounds identified imidazopyrazine compounds as potent inhibitors of *C. parvum* growth (11). This class of imidazopyrazines inhibits phosphatidylinositol 4 kinase (PI4K) in *Plasmodium falciparum* (12), an activity that may explain its potent ability to control *C. parvum* growth *in vitro* and *in vivo*. Prior studies have identified benzoxaboroles that act on mRNA polyadenylation in *P. falciparum* (13), and genetic evidence supports a similar target in *Toxoplasma gondii* (14). Related benzoxaboroles are potent inhibitors of *C. parvum* growth in an *in vitro* model and calf model of cryptosporidiosis (15). Previous studies in *P. falciparum* have also highlighted the potency of bicyclic azetidines that inhibit parasite phenylalanine-tRNA synthetases (PheRS) (16), suggesting that these may also have broad-spectrum activity against other apicomplexans. Consistent with this prediction, recent studies indicate that bicyclic azetidines are also potent inhibitors of *C. parvum* growth *in vitro* (17).

The majority of studies that have identified new inhibitors have utilized microtiter plate-based growth assays that do not rely on knowledge of specific targets. To better understand their mode of action, it would be beneficial to develop assays that identify when compounds act across the life cycle and to define the minimum concentration and time required to achieve complete killing *in vitro*. Deconvolving the targets of activity within the life cycle has been a major focus of successful efforts to define new compounds that inhibit *Plasmodium* spp. (18). Limitations in culturing *C. parvum in vitro* have made it difficult to perform similar studies, although methods have recently been described for staging the activity of inhibitors in tumor cell lines, where partial development takes place (17).

Cryptosporidium spp. undergo their entire life cycle in a single host, consisting of several rounds of asexual amplification followed by sexual differentiation and fertilization to form an oocyst (19). *C. parvum* can be propagated for several rounds of asexual growth in a variety of tumor cell lines *in vitro*, and although it develops into gametocytes, it does not complete the sexual cycle to form oocysts. Thus, only short-term propagation is possible in these systems (20). Recent efforts have developed new platforms to alleviate this restriction and have led to organoid-based systems that use human stem cell-derived cultures to propagate *C. parvum* and to produce oocysts that are infectious to mice (21). However, this system requires microinjection of parasites and does not allow ready access for experimental manipulation. As an alternative system for long-term propagation of *C. parvum*, we have recently described a mouse enterocyte model that is based on the propagation of intestinal stem cells, followed by differentiation on two-dimensional (2D) transwell filters (22, 23). Removal of the liquid medium from the upper chamber to create an air-liquid interface (ALI) induces differentiation of intestinal cell lineages and favors the growth of *C. parvum* (22, 23). Importantly, the ALI culture system is amenable to adding compounds for defined intervals of treatment, and because transwells are grown in microtiter plates, the system can be scaled easily to evaluate multiple parallel cultures.

Here, we sought to examine several newly identified compounds that are potent

TABLE 1 EC_{50} and EC_{90} values for compounds against *C. parvum* grown in HCT8 versus ALI cultures

Compound	EC_{50} (μM) in (mean ± SD):		Fold change[c]	EC_{90} (μM) in (mean ± SD):	
	HCT8 cells[a]	ALI cells[b]		HCT8 cells[a]	ALI cells[a]
Nitazoxanide	2.190 ± 0.378	25.940 ± 4.137	11.8	6.497 ± 2.632	49.250 ± 26.110
KDU691	0.053 ± 0.019	0.132 ± 0.022	2.5	0.164 ± 0.069	0.392 ± 0.130
BRD7929	0.033 ± 0.009	0.113 ± 0.015	3.4	0.225 ± 0.041	0.847 ± 0.264
BRD8494	0.011 ± 0.003	0.028 ± 0.002	2.5	0.081 ± 0.019	0.055 ± 0.020
AN7973	0.347 ± 0.129	0.633 ± 0.359	1.8	1.378 ± 0.500	0.778 ± 0.205
MMV665917	2.360 ± 0.643	3.607 ± 0.944	1.5	9.543 ± 3.568	7.540 ± 2.649

[a]$n = 3$; 9-point (pt) curve. Calculated as log(inhibitor) versus normalized response – variable slope. The assay is based on 24 h of growth.
[b]$n = 2$; 5-pt curve. Calculated as log(inhibitor) versus normalized response – variable slope. The assay is based on 48 h of growth.
[c]Fold change is defined as the ALI-EC_{50} divided by the HCT8-EC_{50}.

inhibitors of *C. parvum* growth *in vitro*. We were interested in defining the window of development when inhibitors are active across the life cycle. We took advantage of the fact that the cycle is somewhat synchronous in HCT-8 adenocarcinoma cells, combined with newly defined antibodies (24) and gene probes for defining the stages of the life cycle, to profile when inhibitors show peak activity. We also used the long-term ALI cell culture to define time- and concentration-dependent conditions required for cidal activity. Together, these tools provide a defined set of reagents and assays for profiling compounds that inhibit *C. parvum in vitro* and help establish guidelines for achieving effective control *in vivo*.

RESULTS

Efficacy of selected anti-*Cryptosporidium* compounds *in vitro*. We focused our study on four classes of potent anti-*Cryptosporidium* compounds identified in previous screening efforts, bicyclic azetidines BRD7929 and BRD8494, the imidazopyrazine KDU691, the benzoxaborole AN7973, and the piperazine MMV665917. To confirm their efficacy with our *C. parvum* strain, AUCP-1, we performed dose-curve assays in HCT-8 cells using a medium-throughput imaging assay (see Materials and Methods) and calculated their respective 50% and 90% effective concentration (EC_{50} and EC_{90}, respectively) values from three independent experiments (Table 1). To determine whether the compounds would be effective under conditions that better mimic the parasite's natural niche, we performed similar dose-response curves in an ALI system that allows long-term cultivation of *C. parvum in vitro* (22, 23). Briefly, mouse ileal stem cell spheroids were plated in transwells on top of an irradiated fibroblast feeder cell layer (Fig. 1A). Monolayers were cultured in conditioned medium (CM) (25–27) for 7 days, at which point the top medium was removed to form the air-liquid interface and promote differentiation of the monolayers. Oocysts were added to the monolayers 3 days after removal of the top medium, and serial dilutions of the compounds were added to the top and bottom chambers of the transwell. After 48 h of compound treatment, EC_{50} and EC_{90} values were calculated based on the number of *C. parvum* genome equivalents in each transwell as quantified by quantitative PCR (qPCR). Even though the times of treatment between the two assays differed (24 h for HCT-8 cells versus 48 h for ALI cultures), all compounds showed a $<$4-fold change in EC_{50} values between the two systems, except for nitazoxanide, which was $\sim$12-fold less potent against *C. parvum* in ALI than in HCT-8 cultures (Table 1).

Reversibility of compound effects on *C. parvum* infection during long-term culture. Although assays to test the cidal versus static properties of compounds against *C. parvum* in HCT-8 cells have been described (8), the lack of *C. parvum* growth after the first 72 h in transformed cell lines limits the ability of these assays to test parasite recovery after compound removal. Thus, we performed washout experiments in our long-term ALI culture system to determine whether treatment with compounds for 48 h was sufficient to kill *C. parvum* or if parasite growth would resume after compound removal during a 72-h recovery period (Fig. 1B). Each compound was tested at three different concentrations (EC_{50}, EC_{90}, and 3$\times$ the EC_{90} for ALI conditions; Table 1) to see

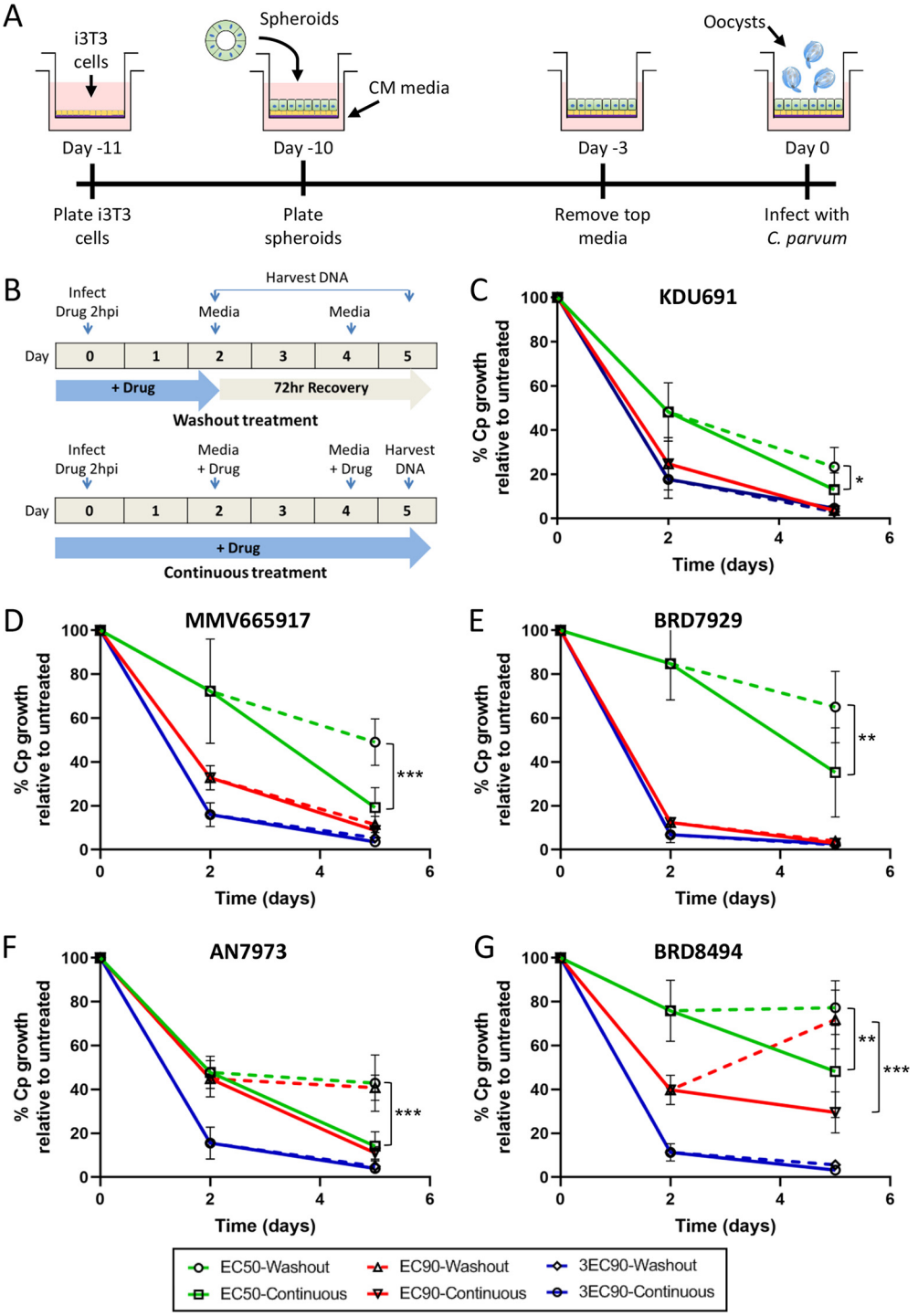

FIG 1 Testing time-dependent killing of *C. parvum* by compounds under air-liquid interface (ALI) culture conditions. (A) Mouse intestinal spheroids were trypsinized and plated on top of irradiated 3T3 (i3T3) feeder cells and Matrigel. The culture was grown in 50% conditioned medium (CM) containing 10 μM ROCK inhibitor. On day 7, medium from the top chamber of the transwell was removed to create the air-liquid interface. Samples were infected 3 days post-medium removal. (B) Compounds were added 2 hpi to transwell monolayers (top and bottom compartments). The transwells were treated with compound for 48 h (washout treatment) or for the entire length of the experiment (5 days) in parallel wells. DNA was harvested at 0, 2, and 5 days postinfection. (C to G) For KDU691 (C), MMV665917 (D), BRD7929 (E), AN7973 (F), and BRD8494 (G) washout experiments, *C. parvum* genome equivalents were quantified using qPCR and normalized to a no-compound control for each time point. Each compound was tested at its ALI EC_{50} (green), EC_{90} (red), and 3× the EC_{90} (blue), with parasite recovery after washout represented by dashed lines and continuous treatment represented by solid lines. Data represent the mean ± standard deviation (SD) for four separate replicate wells from two independent experiments. Statistical analysis was performed using two-way ANOVA corrected for multiple comparisons by Sidak's method. *, $P < 0.05$; **, $P < 0.01$; ***, $P < 0.001$.

whether recovery dynamics changed as the concentration of compound increased. Due to the much less potent activity of nitazoxanide in ALI culture (Table 1), it was not included in these washout assays.

There was significant recovery in parasite growth for all compounds at their respective EC_{50}s after washout versus continuous treatment (Fig. 2C to G). Since the EC_{50}, by definition, would be expected to inhibit only 50% of growth after 48 h of treatment, it was not surprising to see recovery in parasite numbers after washout. However, some compounds were more reversible than others at their respective EC_{50}; KDU691 only showed an ~10% recovery in parasite numbers in washout transwells versus continuous treatment (Fig. 1C), whereas MMV665917 and BRD8494 both demonstrated an ~30% recovery in growth after washout (Fig. 1D and G). Interestingly, parasite growth was irreversible following washout for KDU691, MMV665917, and BRD7929 at their respective EC_{90}s (Fig. 1C to E), while AN7973 and BRD8494 showed significant recovery after washout at the EC_{90} (Fig. 1F and G). However, no compound exhibited recovery after washout at its respective 3× EC_{90} value (Fig. 1C to G), indicating that all compounds are parasiticidal at higher concentrations. Most compounds were not toxic to ALI cultures even at 3× the EC_{90}, with the exception of MMV665917 that showed reduced host cell viability at this concentration (see Fig. S1 in the supplemental material).

Delineating life cycle progression of *C. parvum* in HCT-8 cells. The differences in reversibility at defined potency suggests that the compounds have different mechanisms of inhibiting *C. parvum* growth. To determine if they target different life cycle stages of the parasite, we developed microscopy-based assays to examine the timing of inhibition (Fig. 2A). In both HCT-8 and ALI cultures, *C. parvum* undergoes asexual development and formation of gamonts; however, fertilization is blocked in HCT-8 cultures (20), while it proceeds to oocyst development in ALI cultures (22). To determine the stage against which each compound is most active, we developed methods to define the proportion of each stage present at defined time points during infection. We performed these experiments in HCT-8 cells since the infection is easier to synchronize and visualize by immunofluorescence (IF) microscopy. Infections were synchronized by infection with excysted sporozoites for 2 h and then washing the cultures twice to remove extracellular parasites. Starting 6 hours postinfection (hpi), the thymidine analog EdU was added to cultures in 2-h intervals over a 48-h infection window. Following the EdU pulse, cells were fixed and labeled with an anti-*C. parvum* antibody (referred to as anti-Cp or Cp), and EdU incorporation into parasite DNA was visualized using click chemistry. Parasites were manually counted for each time point and binned into life stages based on the following criteria: those with a single nucleus were classified as trophozoites (Fig. 2B); type I meronts had either 2 nuclei (Fig. 2C), 4 EdU^+ nuclei (Fig. 2D), or 8 nuclei (Fig. 2E); type II meronts had four EdU^- nuclei (Fig. 2F); microgamonts contained more than 8 nuclei (Fig. 2G); and macrogamonts lacked a well-defined nucleus and contained oocyst wall-forming bodies visible by phase contrast microscopy (Fig. 2H).

Trophozoites were exclusively present in the cultures up until 8 hpi; they transitioned to type I meronts by 12 hpi before egressing at 16 hpi and reinvading to commence a second round of asexual merogony that was completed by 24 hpi (Fig. 2I). Type II meronts started appearing as early as 28 hpi and only represented a small fraction of parasites in the culture. However, there are presently no good markers to distinguish between early type I and immature type II meronts, both of which would have four EdU^+ nuclei. Thus, it is possible that our assay underestimates the true number of type II meronts in the culture. Microgamonts appeared around 36 hpi, and macrogamonts with distinguishable wall-forming bodies were visible at ~40 hpi and outnumbered microgamonts by 44 hpi. *C. parvum* gene expression markers confirmed the timing of specific stages in the culture. For example, expression of a transporter gene (cgd2_800) was upregulated at 12 and 20 hpi when type I meronts were most prevalent in the culture but declined over time as gamont differentiation predominated (Fig. 2J). Conversely, the Hap2 gene (cgd8_2220), a microgamont-specific gene that is

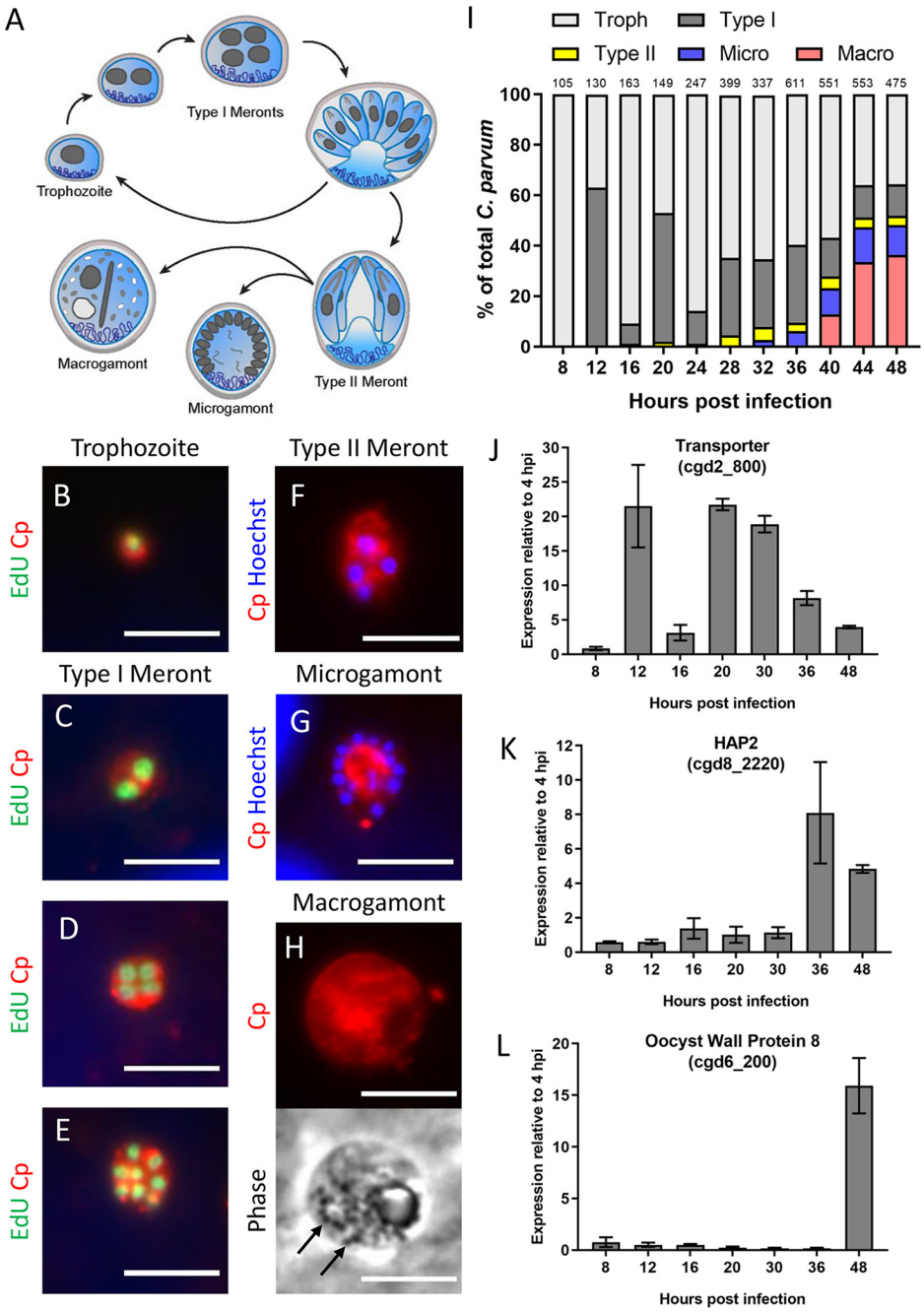

FIG 2 Characterization of *C. parvum* intracellular stages over the first 48 h of infection in HCT-8 cells. (A) Diagram of the *C. parvum* intracellular life cycle. Single-nucleus trophozoites replicate mitotically to form eight mature type I merozoites that egress and reinvade host cells. After at least two rounds of asexual replication, parasites divide into four mature type II meronts, which differentiate into one of two sexual life stages, macrogamonts or multinucleated microgamonts. (B to H) Immunostaining of parasite stages with rabbit polyclonal anti-*C. parvum* (Cp, red) and either EdU, a fluorescent thymidine analog that incorporates into replicating DNA (green), or the nuclear stain Hoechst (blue). Life cycle stages were distinguished as follows: trophozoites, with the presence of a single nuclei (B); type I meronts with the presence of two nuclei C), four EdU$^+$ nuclei (D), or eight nuclei (E); type II meronts with four EdU$^-$ nuclei (F); microgamonts with more than eight nuclei (G); and macrogamonts, with the presence of wall-forming bodies visible by phase contrast (black arrows) (H). Scale bars = 5 μm. (I) Abundance of each life cycle stage as a percentage of total *C. parvum* at the indicated hours postinfection (hpi). For each time point, EdU was added to the culture 2 h prior to fixation and antibody labeling, and the number of parasites at each stage was counted for 10 fields of view with a 100× oil objective. The number of total parasites counted per time point is shown above bar graph. Troph, trophozoites; Macro, macrogamonts; Micro, microgamonts. (J to L) Gene expression of a predicted transporter protein (cgd2_800) (J), the microgametocyte-specific gene HAP2 (cgd8_2220) (K), and a macrogamont oocyst wall protein 8 (cgd6_200) (L) at specified times postinfection with *C. parvum* sporozoites. Gene expression profiles are from a single experiment with three replicates per time point. Values are plotted as the means ± SD.

conserved in male gametes of many eukaryotic species, including *Plasmodium* spp. (28, 29), turned on at 36 hpi when microgamonts started to form (Fig. 2K). Similarly, macrogamont-specific genes such as oocyst wall protein 8 (cgd6_200) were highly expressed 48 hpi when macrogamonts dominated the culture (Fig. 2L).

Determining the effective treatment window for anti-*C. parvum* compounds. To examine the stage(s) in the *C. parvum* life cycle that each compound affected, we performed a sliding window analysis of treatment using the EC_{90} in HCT-8 cells (Table 1 and Fig. 3A). Treatment time windows were chosen to target specific steps in the *C. parvum* life cycle, as summarized in Fig. 3A. Treatment with KDU691 significantly inhibited *C. parvum* growth starting 8 hpi, indicating that it may block merozoite replication or development (Fig. 3C). In contrast, MMV665917 inhibited growth after the first round of asexual merogony was complete, indicating that it may affect parasite egress and/or merozoite reinvasion (Fig. 3D). The compounds that showed the broadest spectrum of stage inhibition were BRD7929 (Fig. 3E) and BRD8494 (Fig. 3F). Both significantly reduced *C. parvum* growth compared to dimethyl sulfoxide (DMSO)-treated controls at almost every time point, indicating that they likely block multiple biological processes or one process shared by multiple stages of parasite development. AN7973 was not active during most of the individual treatment windows and only had a slight, but significant, effect on parasite growth at 28 to 36 hpi (~25% inhibition). In contrast, continuous culture with the compound for the full 48 h inhibited parasite growth by ~85% (Fig. 3B). This indicates that *C. parvum* needs to be exposed to AN7973 for longer than the 4- to 12-h treatment windows in order to be effective. Similarly, treatment with control compound nitazoxanide at the EC_{90} had little effect on parasite growth for most short time points (Fig. S2A); however, such treatment for the full 48 h was completely cytotoxic to the host cells (Fig. S2B). Previous studies have also emphasized the potential toxicity of nitazoxanide, limiting its clinical usefulness (30). None of the other compounds exhibited host toxicity at the EC_{90} over the same time window (Fig. S2B).

EdU pulsing to further dissect the stage specificity of anti-*Cryptosporidium* compounds. We combined EdU pulsing with a monoclonal antibody that labels mature merozoites, 1A5 (24), to better understand the specific biological processes inhibited by each compound. Infected HCT-8 cultures were treated with compounds at the EC_{90}, and EdU was added to individual cultures in 4-h increments until 20 hpi (Fig. 4A). At the end of each 4-h EdU pulse, coverslips were fixed and labeled with 1A5, anti-*C. parvum* (anti-Cp), and click chemistry to label EdU incorporation into newly synthesized DNA. Life cycle stages were then defined based on the number and EdU status of their nuclei and whether the 1A5 marker was present, as follows: trophozoites had one nucleus, early stage meronts had either two or four EdU^+ nuclei, middle meronts had eight EdU^+ nuclei but no 1A5 labeling, and late meronts had eight nuclei and positive 1A5 labeling indicative of merozoite development (Fig. 4B and Fig. S3).

As expected, DMSO control cultures showed a cyclical pattern of DNA replication and merozoite reinvasion, with trophozoites dominating the cultures at 8 hpi and 16 hpi, followed by meronts at 12 hpi and 20 hpi (Fig. 4C). In contrast, KDU691-treated cultures stalled at the late meront stage at 16 hpi, indicating a possible block in merozoite maturation or egress (Fig. 4D). MMV665917-treated cultures lagged in development compared to the DMSO control and still contained a majority of trophozoites at 20 hpi (Fig. 4E). Treatment with BRD7929 completely blocked DNA replication (nearly all parasites contained a single EdU-negative nucleus) up until 20 hpi (Fig. 4F). Last, AN7973-treated cultures showed a lag in development, with fewer parasites continuing to the late meront stage (Fig. 4G). These results were intriguing considering that a recent study reported that AN7973 completely blocked DNA synthesis as detected by a lack of EdU incorporation in compound-treated *C. parvum* (15). This prior study used a higher effective concentration of compound (2× the EC_{90}) and only evaluated a single time point (11 hpi). When we repeated the EdU pulse experiment for AN7973 at both the EC_{90} and 2× the EC_{90}, we found that DNA replication was blocked at the higher concentration until 16 hpi, when ~15% of the parasites had two or more

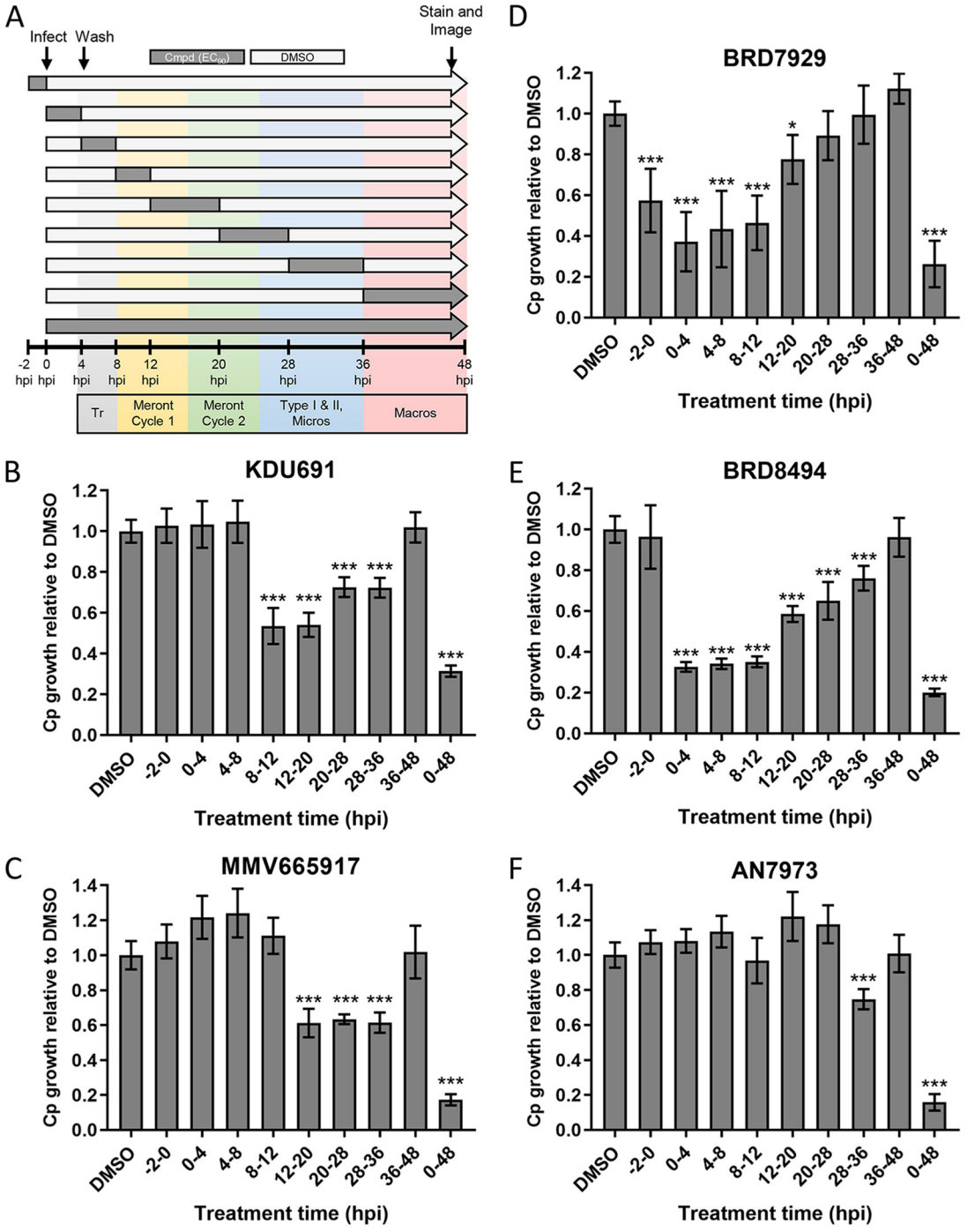

FIG 3 Sliding window analysis of compound effects on different stages of the *C. parvum* life cycle in HCT-8 cells. (A) Diagram of experimental design in which compounds were added at their respective HCT-8 EC_{90}s at specified time intervals (dark gray bars) preinfection (−2 h to 0 h) or postinfection with *C. parvum* oocysts. All wells were washed 4 hpi to remove unexcysted oocysts. After each treatment window, wells were washed then cultured in medium without compound (cmpd) (light-gray bars) for the remainder of the experiment. At 48 hpi, all wells were fixed and labeled with anti-Cp, followed by goat anti-rabbit Alexa Fluor 488. The number of *C. parvum* cells in each well was imaged and counted on a Cytation 3 imager and normalized to DMSO-treated control wells. Approximate timing of *C. parvum* developmental stages is indicated by colored bars. Tr, trophozoites; Micros, microgamonts, Macros, macrogamonts. (B to F) Ratio of Cp growth relative to DMSO controls for AN7973 (B), KDU691 (C), MMV665917 (D), BRD7929 (E), and BRD8494 (F) at their respective EC_{90}s during the indicated time windows postinfection. Each bar represents the mean ± SD for six replicates in total from two independent experiments. Data were analyzed with a one-way ANOVA, followed by Dunnett's multiple-comparison test (*, $P < 0.05$; ***, $P < 0.001$).

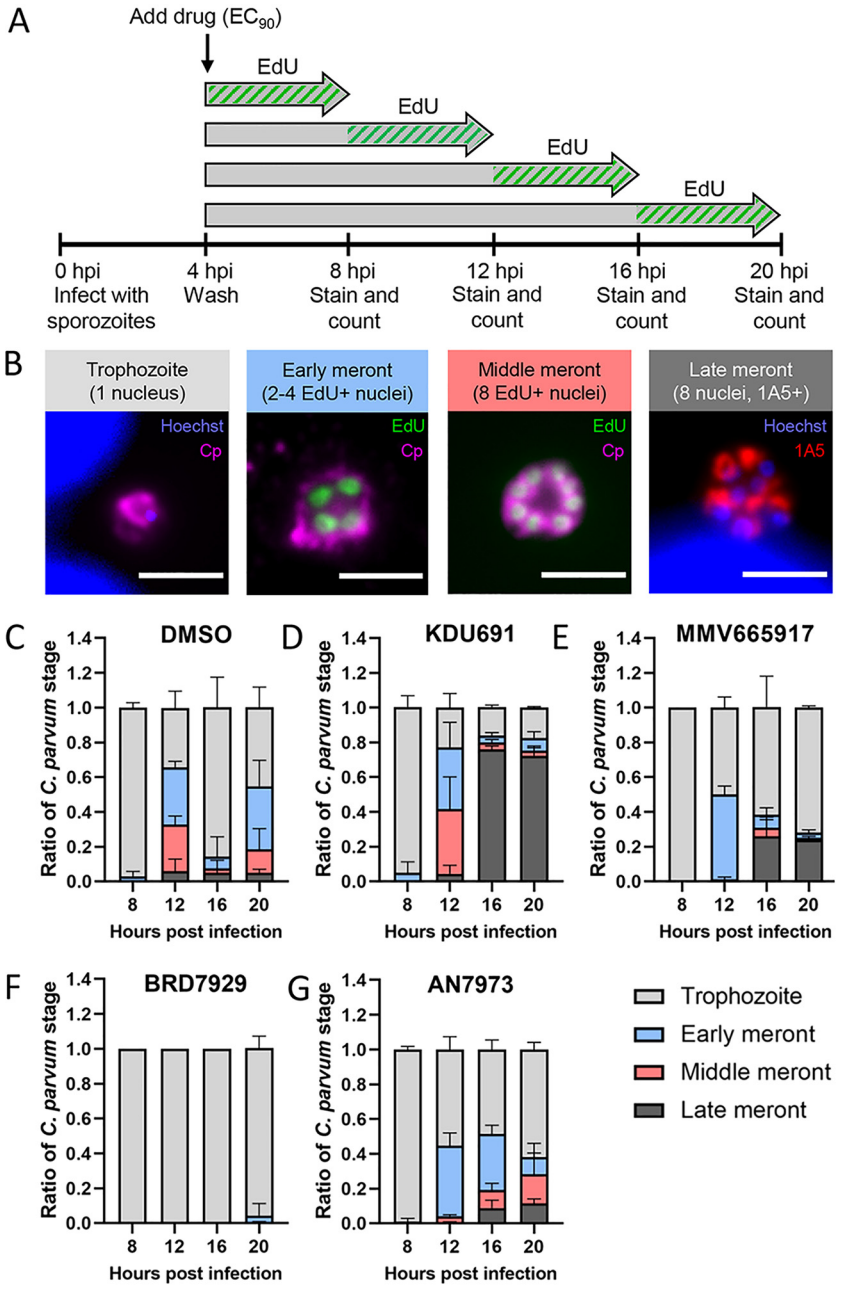

FIG 4 Use of EdU labeling to define effects of compounds on different stages of *C. parvum* asexual replication. (A) HCT-8 cells plated on coverslips were infected with excysted sporozoites for 4 h before compound was added at the EC_{90}. EdU was added to culture medium starting at 4, 8, 12, or 16 hpi. Coverslips were fixed and stained after 4 h of incubation with EdU. (B) Immunofluorescence assay (IFA) images defining the progression of asexual replication using EdU- and stage-specific antibodies. Single-nucleus trophozoites undergo two rounds of DNA replication to form "early meronts" with 2 or 4 EdU^+ nuclei (green). A third round of DNA replication generates "middle meronts" with 8 EdU^+ nuclei, which then mature into "late meronts" containing 8 individual merozoites that each label with monoclonal antibody 1A5 (red) in a polarized manner. Scale bars = 3 μm. (C to G) Quantification of the proportion of each asexual stage present at the indicated time points as defined with EdU and 1A5 labeling for the DMSO control (C), KDU691 (D), MMV665917 (E), BRD7929 (F), and AN7973 (G). Error bars represent the mean ± SD for three biological replicates for each compound and 6 biological replicates for the DMSO control.

EdU^+ nuclei (Fig. S4). Our results corroborate the previous study since we did not detect DNA replication at 12 hpi when treated at 2× the EC_{90}; however, our findings also reveal that some parasites recover at the higher dose given additional time despite constant drug pressure.

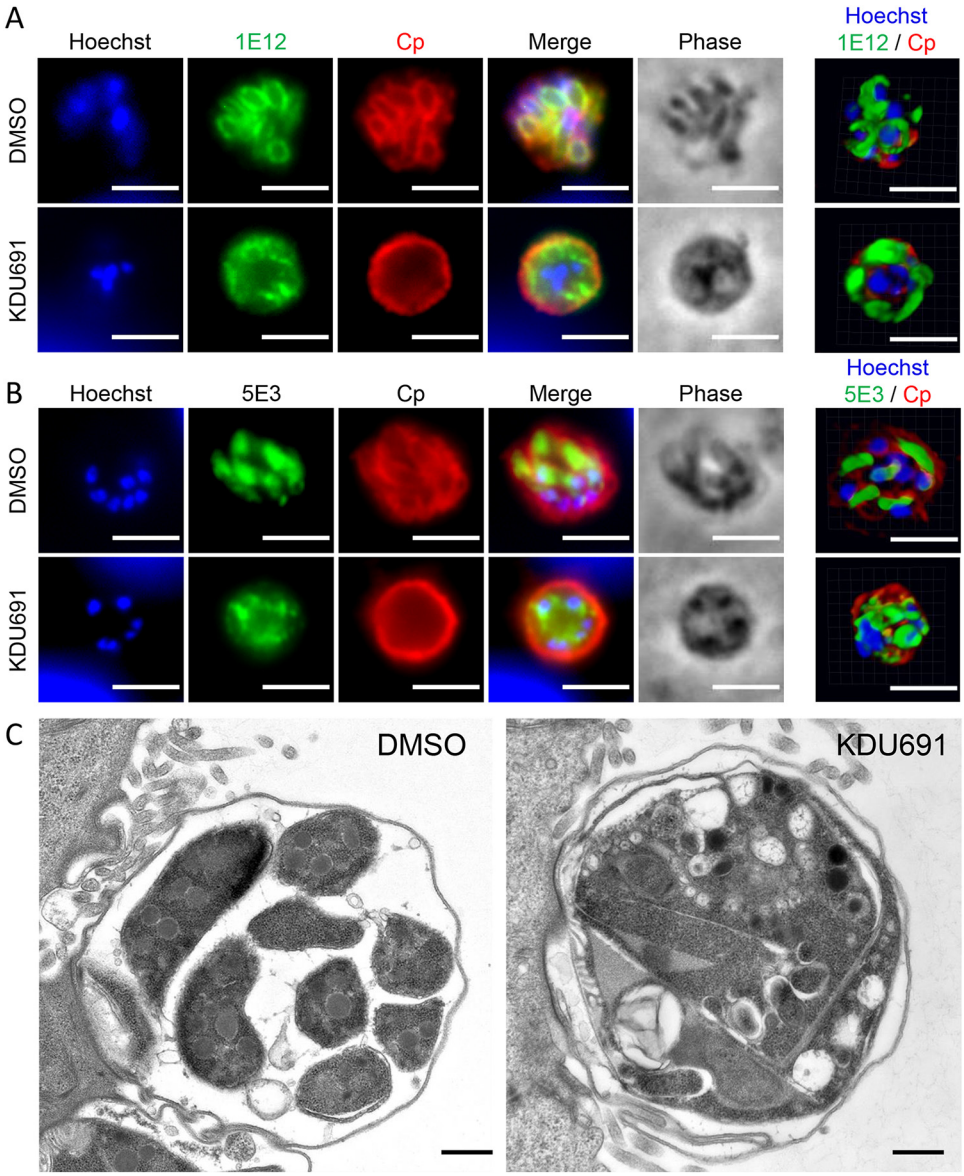

FIG 5 Influence of KDU691 on merozoite maturation. (A and B) IFA images of DMSO- or KDU691-treated parasites from HCT-8 cultures infected with excysted sporozoites fixed and labeled at 22 hpi with anti-Cp (red), Hoechst DNA stain (blue), and either monoclonal antibody 1E12 (green), which localizes to the parasite membrane (A) or monoclonal antibody 5E3, which recognizes the apical end of individual merozoites (B). Images on the right are 3D renderings from confocal z-stacks of parasites labeled with the same antibodies but from independent experiments from the images on the left. Scale bars = 3 μm. (C) Transmission electron micrographs of DMSO- or KDU691-treated parasites at 22 hpi. Scale bars = 500 nm.

KDU691 treatment impedes individual merozoite formation. To further define the block in growth in KDU691-treated cultures, we used immunofluorescence (IF) imaging and transmission electron microscopy (TEM) to examine merozoite development. Monoclonal antibody 1E12, which localizes to *C. parvum* membranes (24), labeled the membranes of individual merozoites in DMSO control cultures at 22 hpi but remained localized around the perimeter of meronts in KDU691-treated cultures (Fig. 5A). Furthermore, monoclonal antibody 5E3, which recognizes the apical pole of excysted sporozoites and individual merozoites in late meronts (24), was detectable at the poles of merozoites in DMSO cultures but showed more diffuse labeling throughout the cytosol in KDU691-treated cultures (Fig. 5B). When examined by electron microscopy, KDU691-treated meronts contained aberrant membrane invaginations and

lacked separate merozoites compared to DMSO control parasites (Fig. 5C). Taken together, these results indicate that KDU691 inhibits merozoite formation, perhaps by impeding the separation of membranes surrounding individual merozoites after DNA replication has occurred. Combined with the accumulation of late-stage meronts as judged by nuclear staining (Fig. 4D), these results indicate that nuclear division is not affected but that egress is likely blocked by the failure of individual merozoites to form in KDU691-treated cultures.

MMV665917 inhibits macrogamont development. Although MMV665917 delayed meront development in the EdU pulse assay (Fig. 4E), there were no obvious defects in merozoite formation based on labeling with 1E12 (Fig. S5A) or 5E3 (Fig. S5B). A previous study found that MMV665917 acted predominantly against the sexual stages of *C. parvum* based on antibody labeling of a meiosis-specific protein, DMC1 (17). To examine macrogamont formation in our cultures, we utilized monoclonal antibody 4D8, which recognizes elongated fibrillar structures in macrogamonts (24). Infected cultures were cultured without compound for 36 hpi to allow for normal asexual development before adding compounds at their respective EC_{90}s for an additional 36 h of culture (Fig. 6A). The labeling pattern of 4D8 was used to quantify the percent inhibition of macrogamont formation after compound treatment. Macrogamonts were considered $4D8^+$ if they showed any striated structure that labeled with 4D8, regardless of length or branching pattern. Macrogamonts treated with KDU691, BRD7929, or AN7973 had 4D8 labeling patterns in both length and branching similar to those in the DMSO control, while $4D8^+$ structures in MMV665917 macrogamonts were much shorter and unbranched (Fig. 6B). When the ratio of macrogamonts to total *C. parvum* was quantified for each compound and expressed as a percentage of inhibition compared to the DMSO control, MMV665917 was the only compound that significantly inhibited the development of $4D8^+$ macrogamonts (Fig. 6C).

BRD7929 treatment blocks nuclear replication and increases feeder organelle area. BRD7929-treated parasites showed a nearly complete block of EdU incorporation (Fig. 4F), suggesting that this compound blocks DNA replication. To test this prediction, we labeled with monoclonal antibody 1B5, which recognizes the base of trophozoites in a unique doughnut pattern (24), at 12 hpi when the type I meronts should be maturing (Fig. 3A). Consistent with this prediction, many parasites in the DMSO control cultures had progressed to the mature type I meront stage, whereas only trophozoites were present in BRD7929-treated cultures (Fig. 7A). Interestingly, we observed expanded 1B5 labeling at the base of BRD7929-treated trophozoites compared to DMSO control cultures when viewed as three-dimensional (3D) renderings of transverse confocal z-stacks through the parasites (Fig. 7B). Since 1B5 likely recognizes an antigen at the host-parasite interface (24), we analyzed infected DMSO- or BRD7929-treated cultures at 12 hpi to determine whether we could observe morphological differences by transmission electron microscopy. To capture parasites with similar orientations from the two treatment groups, we specifically imaged single-nucleus trophozoites sitting on electron-dense pedestals with a sizable host-parasite interface (Fig. 7C). BRD7929-treated trophozoites exhibited normal membrane and nuclear architecture comparable to those from DMSO control cultures (Fig. 7C). However, compound-treated parasites had expanded feeder organelles (Fig. 7C, highlighted in pink) that were significantly larger in area than those from DMSO trophozoites (Fig. 7D). These findings are consistent with BRD7929 blocking parasite replication and stalling growth at the early trophozoite stage.

DISCUSSION

Although several new inhibitors of *Cryptosporidium* sp. growth have been identified in high-throughput screening efforts, we lack good methods for defining their mechanisms of action. To begin alleviating this problem, we have developed several *in vitro* assays to profile the development of life cycle stages that occur *in vitro* and to define static versus cidal activities. Taking advantage of air-liquid interface cultures that allow complete parasite development, we define concentration- and time-dependent treat-

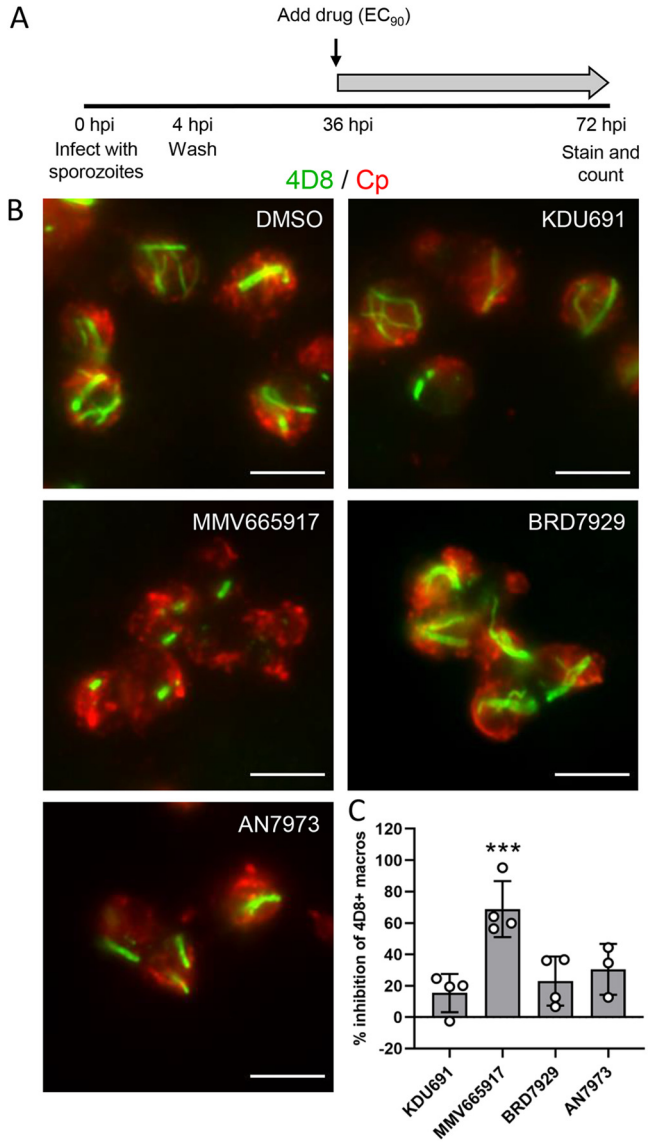

FIG 6 Effect of compounds on formation of macrogamonts. (A) HCT-8 cells plated on coverslips were infected with excysted sporozoites and then washed at 4 hpi to remove extracellular parasites. Compounds were added at their respective EC_{90}s starting at 36 hpi, and cells were fixed and labeled at 72 hpi. (B) IFA images of macrogamonts treated with the indicated compound and labeled with monoclonal antibody 4D8 (green) and anti-Cp (red). Scale bars = 5 μm. (C) Percent inhibition of $4D8^+$ macrogamonts present in cultures treated with the indicated compound compared to DMSO control cultures. Error bars represent the mean ± SD of the results from three independent experiments. Data were analyzed using a nonparametric Kruskal-Wallis test, followed by Dunn's multiple-comparison test that compared each compound to the DMSO control (***, $P < 0.001$).

ment conditions that provide irreversible inhibition. Using a combination of EdU labeling of replicating nuclei and monoclonal antibodies to specific stages, we define the progression of life cycle development that occurs in HCT-8 cells. By combining pulsed compound treatment for defined intervals with EdU pulse labeling, we were able to identify key points in the life cycle that were affected by distinct classes of inhibitors. Among the four classes of compounds studied here were those that block nuclear division (PheRS inhibitors), prevent merozoite formation and hence block egress (PI4K inhibitors), or block macrogamont development (a piperazine inhibitor of unknown function). Collectively, these assays provide a set of guidelines for evaluating future compounds to define the stages of the life cycle that they affect and for defining time- and concentration-dependent killing.

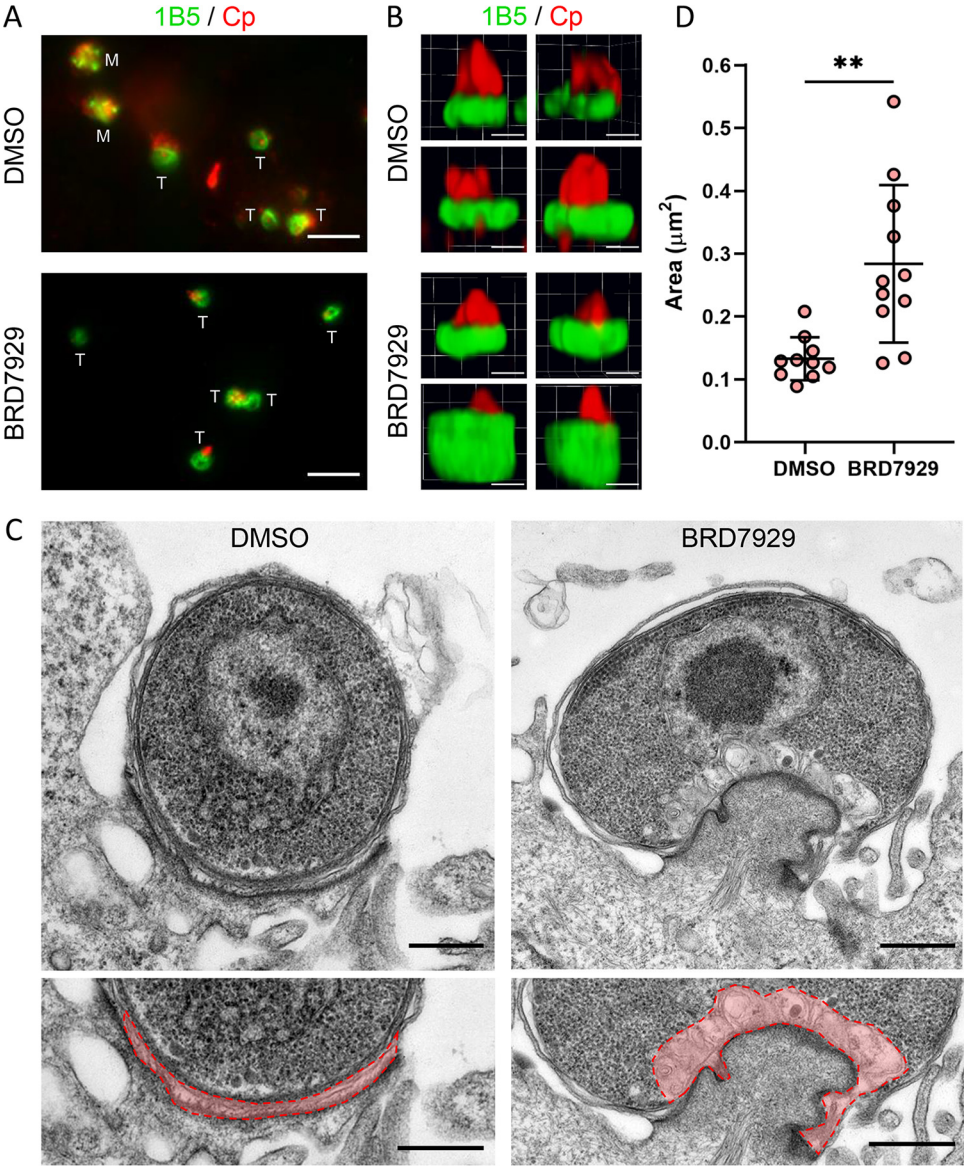

FIG 7 Effect of BRD7929 on parasite replication and formation of the feeder organelle. (A) IFA images of DMSO- or BRD7929-treated parasites from HCT-8 cultures infected with excysted sporozoites fixed and labeled at 12 hpi with anti-Cp (red) and monoclonal antibody 1B5 (green), which localizes to the host-parasite interface. The stages of individual parasites are indicated with "M" for type I meronts or "T" for trophozoites. Scale bars = 5 μm. (B) Three-dimensional renderings from confocal z-stacks of DMSO- or BRD7929-treated parasites from HCT-8 cultures infected with excysted sporozoites fixed and labeled at 8 hpi with 1B5 and rabbit polyclonal anti-Cp (red). Images represent four parasites per treatment group from the same experiment. Scale bars = 1 μm. (C) Transmission electron micrographs of DMSO- or BRD7929-treated parasites at 12 hpi. Bottom images are enlarged sections of the top images with the feeder organelles outlined and false-colored red. Scale bars = 500 nm. (D) Area in μm^2 of the feeder organelles of trophozoites from images from the same experiment as panel C. $n = 10$ trophozoites for DMSO and $n = 11$ trophozoites for BRD7929. Data were analyzed using an unpaired, two-tailed Student t test (**, $P < 0.01$).

One of the limitations of using transformed cell lines such as HCT-8 cells for growing *C. parvum* is that the parasites do not proceed past gamont development (20), and parasite numbers decline over time after reaching a peak between 48 and 72 hpi (31, 32). Although previous studies have tried to estimate "time-to-kill" rates in response to treatment in HCT-8 cells (8, 17), it is not possible to perform classical washout and recovery experiments using such transformed lines due to the fact that replication ceases after a few days. In contrast, *C. parvum* undergoes complete development, including the production of viable oocysts in ALI cultures (22). Moreover, infected ALI

cultures can be propagated for up to 3 weeks (22), providing an experimental system for treatment and recovery experiments. We utilized ALI cultures of *C. parvum* to examine the four classes of compounds studied here using increasing concentrations from the EC_{50}, to the EC_{90}, and to 3× the EC_{90} for a duration of 48 h. All compounds showed partial recovery following treatment at the EC_{50}, a result expected from the fact that this concentration should block growth only by 50%. In contrast, raising the concentration to the EC_{90} resulted in a complete absence of recovery for KDU691, MMV665917, and BRD7929. Somewhat surprisingly, treatment with BRD8494 resulted in partial recovery at the EC_{90}, despite the fact that this compound is very closely related to BRD7929 and likely shares the same PheRS target (16), although this has not been formally demonstrated in *Cryptosporidium* spp. The difference in potency may be a result of the greater hydrophobicity of BRD7929, such that removal by the replacement of medium during the washout phase may be less effective. Additionally, the benzoxaborole AN7973 showed partial recovery even when treated at the EC_{90} and 2× the EC_{90}. This compound was also much less effective than either PheRS or PI4K inhibitors when used for short treatment windows. The longer time requirement for inhibition by AN7973 is consistent with a recent report that estimated the half-life ($t_{1/2}$) for killing to be on the order of 9 h (15). Although we have not extended our studies to *in vivo* treatment, the concentration- and time-dependent findings may be useful in estimating exposure levels that would be needed to achieve complete killing *in vivo*.

A recent study developed a suite of assays for profiling the inhibition of *C. parvum* growth using a combination of cellular assays (17). Here, we extend these assays to examine additional details of the life cycle based on shorter EdU pulses to label replicating nuclei combined with monoclonal antibodies to stage-specific antigens (24). Several of our findings help extend the toolkit for analyzing the life cycle and for deconvolving cellular pathways targeted by different inhibitors. First, the use of short EdU pulses indicates that, in HCT-8 cells, *C. parvum* growth proceeds through two rounds of type I merogony that precedes type II merogony and the appearance of macrogamonts and microgamonts. Second, using antibodies to apical antigens that appear late in merogony (24), we were able to distinguish immature from mature type I meronts as well as type II meronts. It is generally believed that type II meronts give rise to gamonts (33), which makes the low abundance of type II meronts in our cultures surprising given the significant number of gamonts that appear after 36 hpi. However, it is possible that our methods underestimate the true frequency of type II meronts, as there are no known stage-specific markers that are exclusive to type II meronts. Further studies to identify such markers may help resolve this apparent discrepancy. Finally, by using short treatment pulses that were designed to pinpoint distinct life cycle stages, we were able to separate the inhibitor classes in terms of when they are most active.

The compounds BRD7929 and BRD8494, which likely target PheRS, were the most potent in terms of acting rapidly across multiple stages, including preventing nuclear division and thus blocking type I merogony development. In contrast, KDU691, which likely targets PI4K, and MMV665917, which acts on an unknown target, had almost no effect on replicating type I meronts and were only effective when added later in the cycle at the boundary of type I/type II merogony or as sexual stages emerge. By further dissecting the development of type I merogony, it was evident that KDU691 resulted in accumulation of a late-stage type I meront, while the BRD7929 completely blocked nuclear division, arresting parasites at the early trophozoite stage. Finally, both AN7973 and MMV665917 delay the progression of later stages but do not block DNA replication.

By extending our analysis to use monoclonal antibodies that recognize specific structures in the parasite that help define the life cycle, combined with transmission electron microscopy to examine the cellular ultrastructure, we were able to confirm the findings described above and provide a cellular context for understanding the different mechanisms of individual compounds. For example, labeling with antibodies that recognize the apical pole in mature merozoites revealed that KDU691 prevents the separation of merozoites into individual daughter cells. A similar finding has been described previously for *P. falciparum*, where treatment with a related imidazopyrazine

led to multinucleate schizonts that failed to segment into merozoites (12). Consequently, it is likely that KDU691 prevents the egress of merozoites from type I meronts, thus stalling the cycle at this asexual replicating phase. In contrast, MMV665917 has no effect on merozoite division, and fully functional type I meronts are formed, although they are slightly delayed in development. However, the major effect of MMV665917 appears to be aberrant macrogamont formation, as revealed by labeling with monoclonal antibody (MAb) 4D8 that detects a striated fiber that forms in macrogamonts (24). Our finding corroborates a previous report that reached a similar conclusion using a different antibody to macrogamonts (17). However, pulsed treatments with MMV665917 at earlier time points also decreased the number of asexual parasites, indicating that this compound acts on both asexual and sexual development in *C. parvum*. As the target of MMV665917 is unknown, further work is needed to determine whether it targets multiple pathways that independently inhibit asexual and sexual stages or a single pathway shared between the two stages. Finally, the most potent compound that we examined was BRD7929, which completely blocked parasite replication, stalling the parasite at the trophozoite stage. This bicyclic azetidine likely targets PheRS based on studies conducted in *P. falciparum* (16), suggesting that it prevents the synthesis of proteins critical for DNA replication. Treated parasites remain intact for 20 hpi, and the only morphological defect that they displayed was an enlarged feeder organelle, a highly membranous region at the host-parasite interface that is thought to be responsible for the transport of nutrients (34, 35). The enlargement of the feeder organelle suggests that some functions may persist in treated parasites (i.e., transport) despite the block in replication. Nonetheless, treatment with BRD7929 was effective when given for short time intervals, and, when treated for 48 h at the EC_{90}, parasites did not recover from treatment, indicating that the compound is cidal under these conditions.

Cryptosporidiosis has recently been recognized as an important cause of diarrheal disease in infants in the developing world (3, 36). Treatment is limited by the fact that the only existing FDA-approved drug, nitazoxanide, is not approved for infants, is not effective in immunocompromised patients (37), and has varied efficacy in immunocompetent individuals (38). As such, there has been a concerted effort to identify new compounds that are potent and selective inhibitors of *Cryptosporidium* sp. growth as potential leads for the development of new drugs (39). To contribute toward this goal, we have developed methods that can be used to define cidal activity. Importantly, this outcome varies with the concentration and time of treatment that is necessary to prevent the recovery of parasite growth, parameters that are more easily monitored in long-term ALI cultures that support continuous parasite growth. We also expand the repertoire of probes for determining the life cycle stages where compounds are most effective, revealing several novel modes of action among existing lead compounds. These tools should aid future studies evaluating differences in potency, selectivity, mechanism of action, and potential synergy when establishing metrics to achieve *in vivo* efficacy of new drugs for the treatment of cryptosporidiosis.

MATERIALS AND METHODS

Preparation of oocysts. *C. parvum* oocysts were obtained from the Witola lab (University of Illinois at Urbana-Champaign). The *C. parvum* isolate (AUCP-1) was maintained by repeated passage in male Holstein calves and purified from fecal material, as described previously (40). Animal procedures were approved by the Institutional Animal Studies Committee at the University of Illinois at Urbana-Champaign.

Purified oocysts were stored at 4°C in phosphate-buffered saline (PBS) plus 50 mM Tris and 10 mM EDTA (pH 7.2) for up to 6 months. Before infection, *C. parvum* oocysts were treated in a 40% bleach solution (commercial bleach containing 8.25% sodium hypochlorite) diluted in Dulbecco's phosphate-buffered saline (DPBS; Corning Cellgro) for 10 min on ice. Oocysts were then washed three times in DPBS containing 1% (wt/vol) bovine serum albumin (BSA; Sigma) before storing at 4°C in DPBS containing 1% BSA for up to 2 weeks before infection. For some experiments, oocysts were excysted in 0.75% sodium taurocholate at 37°C for 1 h. The excysted sporozoites were centrifuged at 2,500 rpm for 3 min and then resuspended in culture medium prior to use.

Compounds. Previously characterized inhibitors of *C. parvum* growth were obtained from the following organizations: compound MMV665917 was obtained from the University of Vermont, com-

pound AN7973 was obtained from Calibr, compound KDU691 was obtained from Novartis, and compounds BRD7929 (full name, BRD-K78727929-001-03-2) and BRD8494 (full name, BRD-K21118494-001-01-1) were obtained from the Broad Institute. Compounds were dissolved at 10 mM in DMSO and stored at −80°C until use. For use in biological assays, compounds were diluted in culture medium to a final concentration of 1% DMSO and compared to medium containing only 1% DMSO as a control.

HCT-8 cell culture. Human ileocecal adenocarcinoma cells (HCT-8 cells; ATCC CCL-244) were maintained in RPMI 1640 medium (Gibco, ATCC modification) supplemented with 10% fetal bovine serum. Cells were confirmed to be mycoplasma free with the e-Myco plus *Mycoplasma* PCR detection kit (Boca Scientific).

EC_{50} determination in HCT-8 cells. HCT-8 cells plated on 96-well optically clear plates (Greiner Bio-one 655090; Fisher) were infected with oocysts the day after cells reached confluence. Compounds were added in culture medium containing 1% DMSO to generate a 9-point dilution curve to determine their EC_{50} values. Twenty-four hours after compound addition, samples were fixed in 4% formaldehyde for 10 min, washed twice with PBS, permeabilized, and blocked in 0.1% Triton X-100 and 1% BSA in PBS. Samples were labeled with rabbit anti-Cp antibody developed against *C. parvum* oocysts and sporozoites (22), followed by goat anti-rabbit Alexa Fluor 488 (A11034; Invitrogen) in blocking buffer and incubated for 1 h at room temperature, washed three times with buffer, and stained with 1 μg/ml Hoechst for 10 min. Plates were imaged using a BioTek Cytation 3 cell imager to quantify parasite growth (Alexa Fluor 488 label) and monitor host cell viability (Hoechst nuclear staining). EC_{50} and EC_{90} values were calculated using a nonlinear regression curve fit (log inhibitor versus normalized response – variable slope) with three technical replicates per experiment using the Prism 8 software (GraphPad). The mean EC_{50} and EC_{90} per compound are expressed as average values from three independent experiments.

Air-liquid interface culture. The conditions for generating the ALI monolayer system have been defined in greater detail previously (23). Irradiated 3T3 mouse fibroblast (i3T3) cells were plated on transwells (polyester membrane, 0.4-μm pore; Corning Costar, with 12 transwells per 24-well plate) coated with 10% Matrigel (Corning) at a density of 8×10^4 i3T3 cells per transwell. DMEM-high-glucose medium supplemented with 10% fetal bovine serum, 100 U/ml penicillin, and 0.1 mg/ml streptomycin was added to the top (200 μl) and bottom (400 μl) of the transwells and incubated at 37°C for 24 h. Mouse intestinal epithelial cell (mIEC) spheroids were trypsinized and plated on the i3T3 feeder layer the next day (5×10^4 mIECs per transwell). The medium was then changed to 50% L-WRN conditioned medium (CM) supplemented with 10 μM Y-27632 (ROCK inhibitor), as defined previously (25, 26), at the same volumes mentioned above. The 50% CM plus ROCK inhibitor medium was used for the maintenance of ALI transwells, with transwells receiving fresh top medium (200 μl) and bottom medium (400 μl) every 2 to 3 days. After 7 days, medium from the top compartment was removed to initiate the ALI culture, while the bottom medium was changed every 2 to 3 days to maintain the culture.

EC_{50} determination and washout experiments in ALI cultures. ALI monolayers were infected with oocysts on day three after top medium removal and washed at 2 hpi, and a 5-point dilution series of compounds was added to both the top (50 μl) and bottom (400 μl) chambers of the transwell. DNA extraction was performed at 48 h postinfection with the QIAamp DNA minikit (Qiagen). *C. parvum* growth and host cell viability were tracked by monitoring the expression of their respective glyceraldehyde-3-phosphate dehydrogenase (GAPDH) genes using qPCRs that were run on the QuantStudio 3 real-time PCR system (Thermo Fisher), as described previously (22). EC_{50} and EC_{90} values were calculated using a nonlinear regression curve fit (log inhibitor versus normalized response – variable slope) with two technical replicates per experiment using the Prism 8 software (GraphPad). The mean EC_{50} and EC_{90} values per compound are an average of the values from two independent experiments.

ALI monolayers were also used to monitor recovery after treatment with different concentration of compounds. ALI transwells were infected with oocysts on day three after top medium removal and washed at 2 hpi with DPBS, 50 μl of the compound in 50% CM was added to the top of the monolayer, and 400 μl of the compound in 50% CM was added to the bottom chamber. At 48 hpi, transwells were washed three times with DPBS, and the medium was replaced without compound (50 μl top and 400 μl bottom) for the remaining duration of the experiment. For continuous treatments, medium replacement included fresh compound. DNA extraction was done at 2 dpi and 5 dpi using the QIAamp DNA minikit (Qiagen). *C. parvum* and host genome qPCRs were analyzed on the QuantStudio 3 real-time PCR system (Thermo Fisher), as described previously (22), using the QuantStudio software. Two replicates from two independent experiments ($n = 4$) were combined for statistical analysis.

EdU pulsing to define *C. parvum* life cycle progression in HCT-8 cells. To reduce the amount of EdU uptake by replicating host cells, HCT-8 cells from confluent cultures were irradiated at 6,000 rad and stored in liquid nitrogen until further use. Thawed irradiated HCT-8 cells were plated on round coverslips in 24-well culture plates and incubated for ~24 h. HCT-8 monolayers were infected with excysted sporozoites and washed two times with sterile DPBS at 2 hpi to remove extracellular parasites. Starting at 6 hpi, EdU was added to the culture medium at a final concentration of 10 μM for separate 2-h pulses spaced over 48 h before fixing the cells in 4% formaldehyde for 10 min. Coverslips were permeabilized in 0.05% saponin and treated with the Click-iT Plus EdU 488 imaging kit (Thermo Fisher Scientific) to label EdU. Coverslips were then labeled with anti-RH (a polyclonal antibody generated against *Toxoplasma gondii* that recognizes all intracellular stages of *C. parvum* [24]), followed by labeling with Alexa Fluor 568 antibody (Thermo Fisher Scientific) and Hoechst staining. To calculate the percentage of parasites in each life stage per time point, the number of parasites at each life stage was counted from 10 fields using a 100× oil immersion objective on a Zeiss Axioskop Mot Plus fluorescence microscope, and then the sum was divided by the total number of *C. parvum* parasites for that time point.

Analysis of *C. parvum* gene expression. HCT-8 cells were plated in 6-well culture plates and incubated ~24 h before infection. Monolayers were infected with excysted sporozoites, washed twice with DPBS at 2 hpi, and returned to culture in fresh HCT-8 medium. RNA was collected from three wells per time point in RLT buffer (Qiagen) plus 1% β - mercaptoethanol, homogenized using a QIAshredder column (Qiagen), and then stored at −80°C until further processing. RNA was extracted using the RNeasy minikit (Qiagen), treated with the DNA-free DNA removal kit (Thermo Fisher Scientific), and converted to cDNA using the SuperScript VILO cDNA synthesis kit (Thermo Fisher Scientific). Reverse transcription-quantitative PCR (RT-qPCR) was run on a QuantStudio 3 real-time PCR system (Thermo Fisher Scientific) with TB Green Advantage qPCR premix (TaKaRa Bio) and the following primers (5′ to 3′): Transporter cgd2_800 (forward, TGAAAGCGATACAGATGATGGT; reverse, GTTTGTAGGGATTAGCTGGTCAA) (41), HAP2 cgd8_2220 (forward, TTGGATTCATTAGGAGAAATTGG; reverse, ATGTTGCTACCCAAGACACAGA) (41), Oocyst wall protein 8 cgd6_200 (forward, TGATATGCCCAGAAGGAG; reverse, TTATCTCCTCTCTAGCAAC GCA) (41), and *C. parvum* 18S (forward, TAGAGATTGGAGGTTGTTCCT; reverse, CTCCACCAACTAAGAACG GCC) (42). Relative gene expression was calculated with the $\Delta\Delta C_T$ method (43) using *C. parvum* 18S rRNA as the reference gene and normalizing expression to the mean expression of that gene at 4 hpi.

Sliding window analysis of compound effects on *C. parvum* in HCT-8 cells. HCT-8 cells were plated on 96-well optically clear plates (Greiner Bio-one 655090; Fisher) and incubated until confluency (~24 h). To test the effect of pretreatment, wells were treated with compounds at their EC_{90}s in medium containing 1% DMSO for 2 h and then washed three times with DPBS before infection with *C. parvum* oocysts. The remaining wells were infected with *C. parvum* oocysts, washed three times with DPBS after 4 h to remove unexcysted oocysts, and returned to culture. Separate wells were treated with compounds at the EC_{90}s in medium containing 1% DMSO for defined time intervals after infection (i.e., 4- or 8-h intervals, or continuous treatment). At 48 h postinfection, cells were fixed in 4% formaldehyde for 10 min and then labeled with rabbit anti-Cp, followed by goat anti-rabbit Alexa Fluor 488 and Hoechst dye. The plate was imaged on the BioTek Cytation 3 cell imager to calculate the number of *C. parvum* parasites (Alexa Fluor 488 signal) and host cells (Hoechst signal) using the Gen 5 software. Experiments represent two biological replicates performed on different days with three technical replicates per biological replicate.

Determining the stage specificity of compound inhibition using EdU pulsing. HCT-8 cells were plated on 12-mm-diameter glass coverslips (Thermo Fisher Scientific) in 24-well tissue culture plates and incubated until confluency (~24 h). Monolayers were infected with excysted sporozoites, washed twice with DPBS at 4 hpi, and treated with compounds at their EC_{90}s (Table 1) in 1% DMSO in HCT-8 medium. For the EdU pulse labeling, one set of two coverslips per treatment group was incubated with 10 μM EdU and then fixed in 4% formaldehyde after 4 h. Fixed cells were permeabilized, processed for click chemistry as described above, and labeled with mouse monoclonal antibody 1A5 labeled with goat anti-mouse Alexa Fluor 568 (Thermo Fisher Scientific), rabbit anti-Cp labeled with goat anti-rabbit Alexa Fluor 647 (Thermo Fisher Scientific), and Hoechst nuclear stain. Coverslips were mounted on glass slides using ProLong glass antifade mountant (Thermo Fisher Scientific) and sealed with nail polish. The number of parasites at each life stage was counted from 10 fields using a 100× oil immersion objective on a Zeiss Axioskop Mot Plus fluorescence microscope, and the sum was divided by the total number of *C. parvum* parasites for that time point. Ratios were averaged across three independent experiments per compound (six total independent experiments for the DMSO control).

Macrogamont inhibition assay. HCT-8 cells were plated on 12-mm-diameter glass coverslips (Thermo Fisher Scientific) in 24-well tissue culture plates and incubated until confluency (~24 h). Monolayers were infected with unfiltered, excysted oocysts (0.75% sodium taurocholate for 1 h at 37°C), washed twice with DPBS at 4 hpi, and cultured in fresh medium in the absence of compound. At 36 hpi, medium was replaced with compounds at their EC_{90}s (Table 1) in HCT-8 medium containing 1% DMSO and incubated for an additional 36 h before fixation at 72 hpi with 4% formaldehyde. Coverslips were labeled with mouse monoclonal antibody 4D8 labeled with goat anti-mouse Alexa Fluor 488 (Thermo Fisher Scientific), rabbit anti-Cp labeled with goat anti-rabbit Alexa Fluor 568 (Thermo Fisher Scientific), and Hoechst stain. The ratio of $4D8^+$ parasites to the total number of *C. parvum* cells was counted for 10 fields of view on a Zeiss Axioskop Mot Plus fluorescence microscope with a 100× oil immersion objective, and the percent inhibition of $4D8^+$ macrogamonts was calculated for each compound relative to the DMSO control for that experiment. The data represent three independent experiments per compound.

Stage-specific antibody labeling and confocal microscopy. HCT-8 cells were plated on 12-mm-diameter glass coverslips (Thermo Fisher Scientific) in 24-well tissue culture plates and incubated until confluency (~24 h). Monolayers were infected with excysted sporozoites, washed twice with DPBS at 4 hpi, and treated with compounds at their EC_{90}s (Table 1) in HCT-8 medium containing 1% DMSO. Coverslips were fixed in 4% formaldehyde for 10 min, permeabilized and blocked in PBS plus 1% BSA and 0.1% Triton-X, and labeled with primary antibodies, namely, mouse monoclonal antibody 1E12, 5E3, or 1B5, and either rabbit anti-Cp or anti-RH. Mouse monoclonal antibodies were labeled with goat anti-mouse Alexa Fluor 488 (Thermo Fisher Scientific), and rabbit polyclonals were labeled with goat anti-rabbit Alexa Fluor 647 (Thermo Fisher Scientific). DNA was stained with Hoechst.

Epifluorescence images were acquired on a Zeiss Axioskop Mot Plus fluorescence microscope with a 100×, 1.4 numerical aperture (NA) Zeiss Plan-Apochromat oil objective and an AxioCam MRm monochrome digital camera. Images were acquired using AxioVision software (Carl Zeiss, Inc.) and manipulated in ImageJ (https://fiji.sc/). Confocal z-stacks were acquired on a Zeiss LSM880 confocal laser scanning microscope with a 63×, 1.4 NA Zeiss Plan-Apochromat oil objective and Airyscan processing using the ZEN 2.1 black edition software. Three-dimensional images were generated using the visualization module of Volocity version 6.3 (Improvision).

Transmission electron microscopy and measurement of feeder organelle area. HCT-8 cells were plated in 6-well culture plates and incubated for ~24 h until confluency. Monolayers were infected with excysted sporozoites, washed twice with DPBS at 4 hpi, and treated with compounds at their EC_{90}s in HCT-8 medium containing 1% DMSO. At 12 hpi, cell monolayers were scraped, pelleted, and fixed for electron microscopy in 2% paraformaldehyde–2.5% glutaraldehyde (Polysciences, Inc., Warrington, PA) in 100 mM sodium cacodylate buffer (pH 7.2) for 2 h at room temperature and then overnight at 4°C. Samples were washed in sodium cacodylate buffer at room temperature and postfixed in 1% osmium tetroxide (Polysciences, Inc.) for 1 h. Samples were then rinsed extensively in distilled water (dH_2O) prior to *en bloc* staining with 1% aqueous uranyl acetate (Ted Pella, Inc., Redding, CA) for 1 h. Following several rinses in dH_2O, samples were dehydrated in a graded series of ethanol and embedded in Eponate 12 resin (Ted Pella, Inc.). Sections of 95 nm were cut with a Leica Ultracut UCT ultramicrotome (Leica Microsystems, Inc., Bannockburn, IL), stained with uranyl acetate and lead citrate, and viewed on a 1200 EX transmission electron microscope (JEOL USA, Inc., Peabody, MA) equipped with an AMT 8 megapixel digital camera and AMT Image Capture Engine V602 software (Advanced Microscopy Techniques, Woburn, MA). To capture parasites with similar orientations between treatment groups, single-nucleus trophozoites were only imaged if a sizeable host-parasite interface with an electron dense pedestal was present. Feeder organelles were manually outlined in each image, and the surface area within the outline was calculated in ImageJ.

Quantification and statistical analyses. All statistical analyses were performed in Prism (GraphPad). A two-way ANOVA corrected for multiple comparisons by Sidak's method was used to compare compound treatments in ALI. For treatments in HCT-8 cells, data were analyzed with a one-way ANOVA (after confirming normality with a Shapiro-Wilk test), followed by Dunnett's multiple-comparison test. For the macrogamont inhibition assay, data were analyzed with a nonparametric Kruskal-Wallis test, followed by Dunn's test for multiple comparisons. Data on the area of feeder organelles were analyzed with a parametric two-tailed, unpaired Student *t* test after confirming normality with a Shapiro-Wilk test.

SUPPLEMENTAL MATERIAL

Supplemental material is available online only.

FIG S1, TIF file, 1.2 MB.

FIG S2, TIF file, 0.3 MB.

FIG S3, TIF file, 0.8 MB.

FIG S4, TIF file, 1.7 MB.

FIG S5, TIF file, 1.3 MB.

ACKNOWLEDGMENTS

We are grateful to the following individuals for providing the compounds used here: Case McNamara and Melissa Love (Calibr at Scripps Research), Eric Easom and Bob Jacobs (formerly from Anacor), Thierry Diagana and Ujjini Manjunatha (Novartis), Eamon Comer and Cindy Hon (the Broad Institute), and Christopher Huston (University of Vermont). We are also grateful to Wandy Beatty, Microbiology Imaging Facility, for assistance with the electron microscopy, William Witola for providing *C. parvum* oocysts, and Stephen Ward, Bill and Melinda Gates Foundation, for his efforts in coordinating the study.

We declare no competing interests.

REFERENCES

1. Feng Y, Ryan UM, Xiao L. 2018. Genetic diversity and population structure of *Cryptosporidium*. Trends Parasitol 34:997–1011. https://doi.org/10.1016/j.pt.2018.07.009.
2. O'Connor RM, Shaffie R, Kang G, Ward HD. 2011. Cryptosporidiosis in patients with HIV/AIDS. AIDS 25:549–560. https://doi.org/10.1097/QAD.0b013e3283437e88.
3. Kotloff KL. 2017. The burden and etiology of diarrheal illness in developing countries. Pediatr Clin North Am 64:799–814. https://doi.org/10.1016/j.pcl.2017.03.006.
4. Amadi B, Mwiya M, Musuku J, Watuka A, Sianongo S, Ayoub A, Kelly P. 2002. Effect of nitazoxanide on morbidity and mortality in Zambian children with cryptosporidiosis: a randomised controlled trial. Lancet 360:1375–1380. https://doi.org/10.1016/S0140-6736(02)11401-2.
5. Amadi B, Mwiya M, Sianongo S, Payne L, Watuka A, Katubulushi M, Kelly P. 2009. High dose prolonged treatment with nitazoxanide is not effective for cryptosporidiosis in HIV positive Zambian children: a randomised controlled trial. BMC Infect Dis 9:195. https://doi.org/10.1186/1471-2334-9-195.
6. Sparks H, Nair G, Castellanos-Gonzalez A, White AC, Jr. 2015. Treatment of *Cryptosporidium*: what we know, gaps, and the way forward. Curr Trop Med Rep 2:181–187. https://doi.org/10.1007/s40475-015-0056-9.
7. Love MS, Beasley FC, Jumani RS, Wright TM, Chatterjee AK, Huston CD, Schultz PG, McNamara CW. 2017. A high-throughput phenotypic screen identifies clofazimine as a potential treatment for cryptosporidiosis. PLoS Negl Trop Dis 11:e0005373. https://doi.org/10.1371/journal.pntd.0005373.
8. Jumani RS, Bessoff K, Love MS, Miller P, Stebbins EE, Teixeira JE, Campbell MA, Meyers MJ, Zambriski JA, Nunez V, Woods AK, McNamara CW, Huston CD. 2018. A novel piperazine-based drug lead for cryptosporidiosis from the medicines for malaria venture open-access Malaria Box. Antimicrob Agents Chemother 62:e01505-17. https://doi.org/10.1128/AAC.01505-17.
9. Stebbins E, Jumani RS, Klopfer C, Barlow J, Miller P, Campbell MA, Meyers MJ, Griggs DW, Huston CD. 2018. Clinical and microbiologic efficacy of the piperazine-based drug lead MMV665917 in the dairy calf cryptosporidiosis model. PLoS Negl Trop Dis 12:e0006183. https://doi.org/10.1371/journal.pntd.0006183.
10. Lee S, Ginese M, Girouard D, Beamer G, Huston CD, Osbourn D, Griggs

DW, Tzipori S. 2019. Piperazine-derivative MMV665917: an effective drug in the diarrheic piglet model of *Cryptosporidium hominis*. J Infect Dis 220:285–293. https://doi.org/10.1093/infdis/jiz105.
11. Manjunatha UH, Vinayak S, Zambriski JA, Chao AT, Sy T, Noble CG, Bonamy GMC, Kondreddi RR, Zou B, Gedeck P, Brooks CF, Herbert GT, Sateriale A, Tandel J, Noh S, Lakshminarayana SB, Lim SH, Goodman LB, Bodenreider C, Feng G, Zhang L, Blasco F, Wagner J, Leong FJ, Striepen B, Diagana TT. 2017. A *Cryptosporidium* PI(4)K inhibitor is a drug candidate for cryptosporidiosis. Nature 546:376–380. https://doi.org/10.1038/nature22337.
12. McNamara CW, Lee MC, Lim CS, Lim SH, Roland J, Simon O, Yeung BK, Chatterjee AK, McCormack SL, Manary MJ, Zeeman AM, Dechering KJ, Kumar TS, Henrich PP, Gagaring K, Ibanez M, Kato N, Kuhen KL, Fischli C, Nagle A, Rottmann M, Plouffe DM, Bursulaya B, Meister S, Rameh L, Trappe J, Haasen D, Timmerman M, Sauerwein RW, Suwanarusk R, Russell B, Renia L, Nosten F, Tully DC, Kocken CH, Glynne RJ, Bodenreider C, Fidock DA, Diagana TT, Winzeler EA. 2013. Targeting *Plasmodium* PI(4)K to eliminate malaria. Nature 504:248–253. https://doi.org/10.1038/nature12782.
13. Sonoiki E, Ng CL, Lee MC, Guo D, Zhang YK, Zhou Y, Alley MR, Ahyong V, Sanz LM, Lafuente-Monasterio MJ, Dong C, Schupp PG, Gut J, Legac J, Cooper RA, Gamo FJ, DeRisi J, Freund YR, Fidock DA, Rosenthal PJ. 2017. A potent antimalarial benzoxaborole targets a *Plasmodium falciparum* cleavage and polyadenylation specificity factor homologue. Nat Commun 8:14574. https://doi.org/10.1038/ncomms14574.
14. Palencia A, Bougdour A, Brenier-Pinchart MP, Touquet B, Bertini RL, Sensi C, Gay G, Vollaire J, Josserand V, Easom E, Freund YR, Pelloux H, Rosenthal PJ, Cusack S, Hakimi MA. 2017. Targeting *Toxoplasma gondii* CPSF3 as a new approach to control toxoplasmosis. EMBO Mol Med 9:385–394. https://doi.org/10.15252/emmm.201607370.
15. Lunde CS, Stebbins EE, Jumani RS, Hasan MM, Miller P, Barlow J, Freund YR, Berry P, Stefanakis R, Gut J, Rosenthal PJ, Love MS, McNamara CW, Easom E, Plattner JJ, Jacobs RT, Huston CD. 2019. Identification of a potent benzoxaborole drug candidate for treating cryptosporidiosis. Nat Commun 10:2816. https://doi.org/10.1038/s41467-019-10687-y.
16. Kato N, Comer E, Sakata-Kato T, Sharma A, Sharma M, Maetani M, Bastien J, Brancucci NM, Bittker JA, Corey V, Clarke D, Derbyshire ER, Dornan GL, Duffy S, Eckley S, Itoe MA, Koolen KMJ, Lewis TA, Lui PS, Lukens AK, Lund E, March S, Meibalan E, Meier BC, McPhail JA, Mitasev B, Moss EL, Sayes M, Van Gessel Y, Wawer MJ, Yoshinaga T, Zeeman A-M, Avery VM, Bhatia SN, Burke JE, Catteruccia F, Clardy JC, Clemons PA, Dechering KJ, Duvall JR, Foley MA, Gusovsky F, Kocken CHM, Marti M, Morningstar ML, Munoz B, Neafsey DE, Sharma A, Winzeler EA, Wirth DF, et al. 2016. Diversity-oriented synthesis yields novel multistage antimalarial inhibitors. Nature 538:344–349. https://doi.org/10.1038/nature19804.
17. Jumani RS, Hasan MM, Stebbins EE, Donnelly L, Miller P, Klopfer C, Bessoff K, Teixeira JE, Love MS, McNamara CW, Huston CD. 2019. A suite of phenotypic assays to ensure pipeline diversity when prioritizing drug-like *Cryptosporidium* growth inhibitors. Nat Commun 10:1862. https://doi.org/10.1038/s41467-019-09880-w.
18. Leroy D, Campo B, Ding XC, Burrows JN, Cherbuin S. 2014. Defining the biology component of the drug discovery strategy for malaria eradication. Trends Parasitol 30:478–490. https://doi.org/10.1016/j.pt.2014.07.004.
19. Tzipori S, Widmer G. 2000. The biology of *Cryptosporidium*. Contrib Microbiol 6:1–32. https://doi.org/10.1159/000060370.
20. Tandel J, English ED, Sateriale A, Gullicksrud JA, Beiting DP, Sullivan MC, Pinkston B, Striepen B. 2019. Life cycle progression and sexual development of the apicomplexan parasite *Cryptosporidium parvum*. Nat Microbiol 4:2226–2236. https://doi.org/10.1038/s41564-019-0539-x.
21. Heo I, Dutta D, Schaefer DA, Iakobachvili N, Artegiani B, Sachs N, Boonekamp KE, Bowden G, Hendrickx APA, Willems RJL, Peters PJ, Riggs MW, O'Connor R, Clevers H. 2018. Modelling *Cryptosporidium* infection in human small intestinal and lung organoids. Nat Microbiol 3:814–823. https://doi.org/10.1038/s41564-018-0177-8.
22. Wilke G, Funkhouser-Jones LJ, Wang Y, Ravindran S, Wang Q, Beatty WL, Baldridge MT, VanDussen KL, Shen B, Kuhlenschmidt MS, Kuhlenschmidt TB, Witola WH, Stappenbeck TS, Sibley LD. 2019. A stem-cell-derived platform enables complete *Cryptosporidium* development in vitro and genetic tractability. Cell Host Microbe 26:123–134.e8. https://doi.org/10.1016/j.chom.2019.05.007.
23. Wilke G, Wang Y, Ravindran S, Stappenbeck T, Witola WH, Sibley LD. 2020. In vitro culture of *Cryptosporidium parvum* using stem cell-derived intestinal epithelial monolayers, p 351–372. In Mead J, Arrowood M (ed), Cryptosporidium methods in molecular biology, vol 2052. Humana Press, New York, NY.
24. Wilke G, Ravindran S, Funkhouser-Jones L, Barks J, Wang Q, VanDussen KL, Stappenbeck TS, Kuhlenschmidt TB, Kuhlenschmidt MS, Sibley LD. 2018. Monoclonal antibodies to intracellular stages of *Cryptosporidium parvum* define life cycle progression in vitro. mSphere 3:e00124-18. https://doi.org/10.1128/mSphere.00124-18.
25. Miyoshi H, Ajima R, Luo C, Yamaguchi TP, Stappenbeck TS. 2012. Wnt5a potentiates TGF-beta signaling to promote colonic crypt regeneration after tissue injury. Science 338:108–113. https://doi.org/10.1126/science.1223821.
26. Miyoshi H, Stappenbeck TS. 2013. In vitro expansion and genetic modification of gastrointestinal stem cells in spheroid culture. Nat Protoc 8:2471–2482. https://doi.org/10.1038/nprot.2013.153.
27. VanDussen KL, Sonnek NM, Stappenbeck TS. 2019. L-WRN conditioned medium for gastrointestinal epithelial stem cell culture shows replicable batch-to-batch activity levels across multiple research teams. Stem Cell Res 37:101430. https://doi.org/10.1016/j.scr.2019.101430.
28. Fédry J, Liu Y, Pehau-Arnaudet G, Pei J, Li W, Tortorici MA, Traincard F, Meola A, Bricogne G, Grishin NV, Snell WJ, Rey FA, Krey T. 2017. The ancient gamete fusogen HAP2 is a eukaryotic class II fusion protein. Cell 168:904–915.e10. https://doi.org/10.1016/j.cell.2017.01.024.
29. Liu Y, Tewari R, Ning J, Blagborough AM, Garbom S, Pei J, Grishin NV, Steele RE, Sinden RE, Snell WJ, Billker O. 2008. The conserved plant sterility gene HAP2 functions after attachment of fusogenic membranes in *Chlamydomonas* and *Plasmodium* gametes. Genes Dev 22:1051–1068. https://doi.org/10.1101/gad.1656508.
30. Mead JR, Arrowood MJ. 2014. Treatment of cryptosporidiosis. In Caccio SM, Widmer G (ed), Cryptosporidium: parasite and disease. Springer, Vienna, Austria.
31. Arrowood MJ. 2002. In vitro cultivation of *Cryptosporidium* species. Clin Microbiol Rev 15:390–400. https://doi.org/10.1128/cmr.15.3.390-400.2002.
32. Upton SJ, Tilley M, Brillhart DB. 1994. Comparative development of *Cryptosporidium parvum* (Apicomplexa) in 11 continuous host cell lines. FEMS Microbiol Lett 118:233–236. https://doi.org/10.1111/j.1574-6968.1994.tb06833.x.
33. Bouzid M, Hunter PR, Chalmers RM, Tyler KM. 2013. *Cryptosporidium* pathogenicity and virulence. Clin Microbiol Rev 26:115–134. https://doi.org/10.1128/CMR.00076-12.
34. Bochimoto H, Kondoh D, Ishihara Y, Kabir MHB, Kato K. 2019. Three-dimensional fine structure of feeder organelle in *Cryptosporidium parvum*. Parasitol Int 73:101958. https://doi.org/10.1016/j.parint.2019.101958.
35. Perkins ME, Riojas YA, Wu TW, Le Blancq SM. 1999. CpABC, a *Cryptosporidium parvum* ATP-binding cassette protein at the host-parasite boundary in intracellular stages. Proc Natl Acad Sci U S A 96:5734–5739. https://doi.org/10.1073/pnas.96.10.5734.
36. Kotloff KL, Nataro JP, Blackwelder WC, Nasrin D, Farag TH, Panchalingam S, Wu Y, Sow SO, Sur D, Breiman RF, Faruque AS, Zaidi AK, Saha D, Alonso PL, Tamboura B, Sanogo D, Onwuchekwa U, Manna B, Ramamurthy T, Kanungo S, Ochieng JB, Omore R, Oundo JO, Hossain A, Das SK, Ahmed S, Qureshi S, Quadri F, Adegbola RA, Antonio M, Hossain MJ, Akinsola A, Mandomando I, Nhampossa T, Acácio S, Biswas K, O'Reilly CE, Mintz ED, Berkeley LY, Muhsen K, Sommerfelt H, Robins-Browne RM, Levine MM. 2013. Burden and aetiology of diarrhoeal disease in infants and young children in developing countries (the Global Enteric Multicenter Study, GEMS): a prospective, case-control study. Lancet 382:209–222. https://doi.org/10.1016/S0140-6736(13)60844-2.
37. Checkley W, White AC, Jr, Jaganath D, Arrowood MJ, Chalmers RM, Chen XM, Fayer R, Griffiths JK, Guerrant RL, Hedstrom L, Huston CD, Kotloff KL, Kang G, Mead JR, Miller M, Petri WA, Jr, Priest JW, Roos DS, Striepen B, Thompson RC, Ward HD, Van Voorhis WA, Xiao L, Zhu G, Houpt ER. 2015. A review of the global burden, novel diagnostics, therapeutics, and vaccine targets for *Cryptosporidium*. Lancet Infect Dis 15:85–94. https://doi.org/10.1016/S1473-3099(14)70772-8.
38. Anderson VR, Curran MP. 2007. Nitazoxanide: a review of its use in the treatment of gastrointestinal infections. Drugs 67:1947–1967. https://doi.org/10.2165/00003495-200767130-00015.
39. Chavez MA, White AC, Jr. 2018. Novel treatment strategies and drugs in development for cryptosporidiosis. Expert Rev Anti Infect Ther 16:655–661. https://doi.org/10.1080/14787210.2018.1500457.
40. Zhang X, Kim CY, Worthen T, Witola WH. 2018. Morpholino-mediated in vivo silencing of *Cryptosporidium parvum* lactate dehydrogenase de-

creases oocyst shedding and infectivity. Int J Parasitol 48:649–656. https://doi.org/10.1016/j.ijpara.2018.01.005.
41. Mauzy MJ, Enomoto S, Lancto CA, Abrahamsen MS, Rutherford MS. 2012. The *Cryptosporidium parvum* transcriptome during in vitro development. PLoS One 7:e31715. https://doi.org/10.1371/journal.pone.0031715.
42. Abrahamsen MS, Schroeder AA. 1999. Characterization of intracellular Cryptosporidium parvum gene expression. Mol Biochem Parasitol 104:141–146. https://doi.org/10.1016/S0166-6851(99)00081-X.
43. Schmittgen TD, Livak KJ. 2008. Analyzing real-time PCR data by the comparative C_T method. Nat Protoc 3:1101–1108. https://doi.org/10.1038/nprot.2008.73.